# The mechanism of dross formation in the hot-dip 55 wt.% Al-Zn-Si coating process

*Qun LUO, Feng JIN, Qian LI, Jieyu ZHANG, Kuochih CHOU*

*Shanghai Key Laboratory of Modern Metallurgy & Materials Processing, Shanghai University, Shanghai 200072, China*

**Abstract:** The dross formation is closely related with the solubility of Fe in the molten bath. When the Fe level exceeds the saturation solubility of liquid, the dross precipitates in the form of intermetallic compounds. Inductively coupled plasma atomic emission spectrometry (ICP) was used to determine the content of Fe in molten bath. The morphology of the bottom dross was observed by scanning electron microscopy (SEM). Based on the experimental results and the calculated phase diagram of the Al-Zn-Si-Fe system, the effects of bath temperature and Si content in the molten bath on the Fe solubility were analyzed, and then the mechanism of dross formation was investigated. The results showed that when the bath temperature decreased from 630 °C to 590 °C, the solubility of Fe in liquid reduced from 0.12 wt.% to 0.06 wt.% and 0.17 wt.% $FeAl_3$ would precipitate from the liquid. Compared with the Fe dissolution lines at different Si content, it can be seen that the solubility of Fe in Al-Zn melt increased with the increasing of Si content from 0.5 wt.% to 1.5 wt.%. However, the amount of precipitated $FeAl_3$ in 55wt.%Al-Zn-1.5Si molten alloy (0.17 wt.%) was greater than that in 55wt.%Al-Zn-0.5Si molten alloy (0.14 wt.%) in the same temperature range. It means that the more the Si contents in the liquid, the greater the amount of dross formation.

**Keywords:** Hot-dip, 55wt. % Al-Zn-Si, dross formation, thermodynamics

## 1. Introduction

Hot dipping coating is a widely used protective coating. The relatively mature developed coating mainly contains three types: Galvalume (55wt.%-Al-43.5Zn-1.5Si) developed by Bethlehem Steel company, Galfan (Zn-5wt.%Al-0.1mesch metal) developed by International Lead and Zinc Research Organization (ILZRO) and Super-Zinc (Zn-4.5wt.%Al-0.1Mg) developed by Nippon Steel corporation. Among those coatings, the most important one is the high aluminum Galvalume (GL) coating [1-3], and it has been widely used in building, automobile, agriculture, household appliances, etc. Although the GL production line has been introduced into domestic in recent years, the study of GL coating was just started. One of the main problems faced by the galvanizing steel industries is the formation of intermetallic compounds (dross) on the surface of the rolls, at the bottom of the pot and frequent stoppage of lines. The formation of bottom dross not only wastes the resource and energy, but also impairs the quality of coating. In addition, salvaging the dross at regular intervals would cause loss in efficiency [4].

The dross in the zinc bath can be divided into floating dross, suspended dross and bottom dross according to

its density. The density of the 55wt.%Al-Zn-Si molten alloy is about 3327 kg/m$^3$ [5]. The floating dross in the molten bath mainly includes some oxide such as zinc oxide and alumina. Owing to the addition of element Al and Si in the plating bath, the phase relationship in 55wt.%Al-Zn-Si molten bath was relatively more complicate than that in pure zinc molten bath. Many research thought that the bottom dross in the 55wt.%Al-Zn-Si melt contained $FeAl_3$ (3850 kg/m$^3$) and Fe-Al-Si intermetallics [6]. The dross formation is closely related with the solubility of Fe in the plating bath. When the Fe level exceeds the saturation solubility of melt, the dross will precipitate in the form of intermetallic compounds. Many factors can affect the solubility of Fe, such as bath temperature [9, 10], alloy element [11, 12] and materials of equipment [10]. However, using the empirical method to study the effect of those factors proved impractical because of the time-consuming process and huge workload. The aim of this research was to investigate the effects of bath temperature and Si content on dross formation based on the thermodynamic calculated phase diagram. Then the control measure of dross formation in 55wt.%Al-Zn-Si bath was put forward.

## 2. Experimental procedures

The experiment was carried out on the homemade hot dipping equipment [13]. The protective atmosphere of zinc bath was 10 vol.% $H_2$ + $N_2$ gas with flowing rate at 20 L/min. In order to make the Fe solution in melt achieve saturated, an overdose of steel sheet was immersed in the 55wt.%Al-Zn-Si molten bath and remain for about 1 h. Many granular ferrous slags were observed at the surface of steel sheet. Then the liquid samples were draw from the bath using long silica tubes at 630, 610 and 590 °C, respectively. The bottom dross was salvaged from the bottom of bath. ICP was applied to determine the content of Al, Zn, Si and Fe in the samples at different temperatures. X-ray diffraction (XRD) was used to analyze the phase compositions of the bottom dross powder. The morphology and chemical compositions of etched dross were investigated by means of JSM-6700 SEM equipped with energy dispersive X-ray spectrometer (EDS).

## 3. Results

Table 1 shows the composition of the molten alloy at different temperatures which determined by ICP. The content of Al, Zn and Si changed not so much. However, the content of Fe in the molten alloy decreased from 0.13 wt.% to 0.08 wt.% when temperature reduced from 630 °C to 590 °C, which indicating that the saturation solubility of Fe decreased with the reduction of temperature.

Table 1. The compositions of the molten alloy at different temperature

| Temperature | Composition/wt.% | | | | |
|---|---|---|---|---|---|
| /°C | Al | Zn | Si | Fe | Others |
| 590 | 54.68 | 43.72 | 1.34 | 0.08 | - |
| 610 | 55.19 | 43.33 | 1.24 | 0.11 | - |
| 630 | 54.86 | 43.46 | 1.38 | 0.13 | - |

The XRD pattern of the bottom dross powders was shown in Fig. 1. Except the (Al) and (Zn) phases the main

phase in dross is $FeAl_3$. In addition, a little $Al_{11}V$ phase existed in. The (Al) and (Zn) phases were formed after the solidification of the liquid. The back scattered electrons image (BSE) of the etched bottom dross was shown in Fig. 2. It can be seen that large grey particles were inlaid in the black reticular matrix. A few white small particles interspersed between the large grey particles. The reticular matrix was the (Al) and (Zn) two phase region which formed by solidification of the liquid at interstitial space between dross particles.

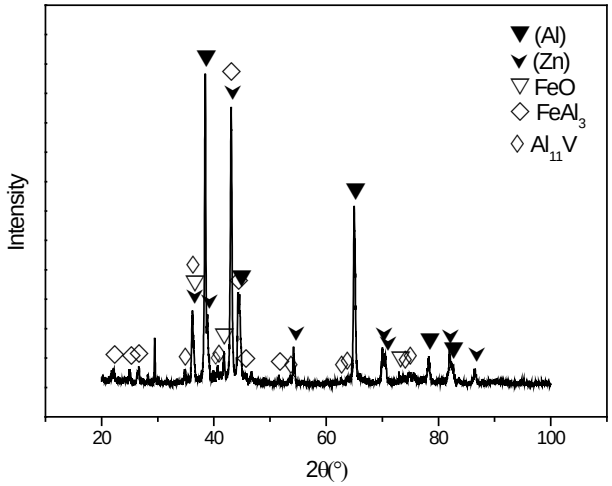


**Fig. 1**. The XRD pattern of the bottom dross

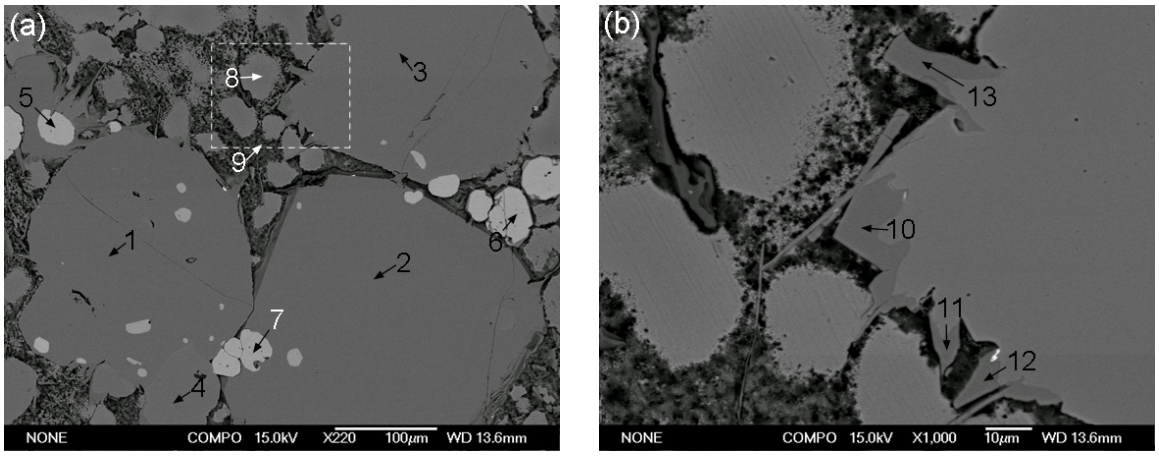


**Fig. 2.** The BSE image of the bottom dross: (a) the overview image of the bottom dross, (b) the enlarged image of bottom dross marked with white dash line in (a)

The compositions of the phases in the bottom dross were determined by EDS and listed in Table 2. The compositions of the large particles (1, 2, 3 and 4) are roughly same and near to the composition of $FeAl_3$ phase. Points 5, 6 and 7 correspond to the small white particles, which contain high content of Al and Zn, and about 6.8 at.% V. It is thought to be a kind of Al-Zn-V compound. Points 8 and 9 are the Al-rich dendrited (Al) and interdendritic (Al)' phases, respectively. When cooling to room temperature, the (Al)' phase was decomposed to (Al) and (Zn) phases. The high content of oxygen at point 9 was due to the oxidization of the interdendritic which caused by etch. The Fig. 2(b) shows the enlarged image of the bottom dross which marked with white dash line in Fig. 2(a). The compositions of points 10, 11, 12 and 13 are near to the composition of β-AlSiFe,

which distribute on the edge of large $FeAl_3$ particle.

**Table 2.** The EDS results of the bottom dross

| No. | Elements/at.% | | | | | | | Phases |
|---|---|---|---|---|---|---|---|---|
| | Al | Zn | Si | Fe | V | Ce | O | |
| 1 | 69.4 | 2.0 | 8.9 | 19.7 | - | - | - | $FeAl_3$ |
| 2 | 67.4 | - | 8.5 | 24.1 | - | - | - | |
| 3 | 69.4 | 4.4 | 6.9 | 19.6 | - | - | - | |
| 4 | 69.6 | 3.7 | 7.0 | 19.7 | - | - | - | |
| 5 | 65.4 | 25.4 | 3.2 | - | 6.0 | - | - | Al-V-Zn |
| 6 | 61.4 | 26.5 | 1.4 | - | 6.0 | 4.7 | - | |
| 7 | 69.2 | 22.5 | - | - | 8.3 | - | - | |
| 8 | 80.2 | 19.8 | - | - | - | - | - | (Al) |
| 9 | 78.7 | 7.6 | - | - | - | - | 13.7 | (Al)+(Zn) |
| 10 | 65.0 | 2.1 | 17.4 | 15.5 | - | - | - | β-AlSiFe |
| 11 | 63.6 | 2.4 | 17.8 | 16.2 | - | - | - | |
| 12 | 64.5 | 2.9 | 16.1 | 16.5 | - | - | - | |
| 13 | 65.9 | 2.6 | 15.7 | 15.8 | - | - | - | |

## 4. Thermodynamic analysis of the dross formation

### 4.1 The effect of bath temperature on solubility of Fe in 55wt.%Al-Zn-Si molten alloy

The isoplethal section of Al-Zn-Si-Fe system from 55wt.%Al-Zn-1.3Si to 55wt.%Al-Zn-1.3Si-1Fe (showed in Fig. 3) was calculated based on Al-Zn-Si-Fe thermodynamic database which constructed by our work group. The boundary between liquid region and liquid+$FeAl_3$ two phase region is the saturation solubility curve of Fe in the molten alloy. It can be seen that the solubility of Fe increased from 0.06 wt.% to 0.12 wt.% with temperature rising from 590 °C to 630 °C. The calculated values of Fe solubility agree with the experimental data. When the content of Fe exceeds the saturation solubility, the $FeAl_3$ phase will precipitate from the liquid and become bottom dross.

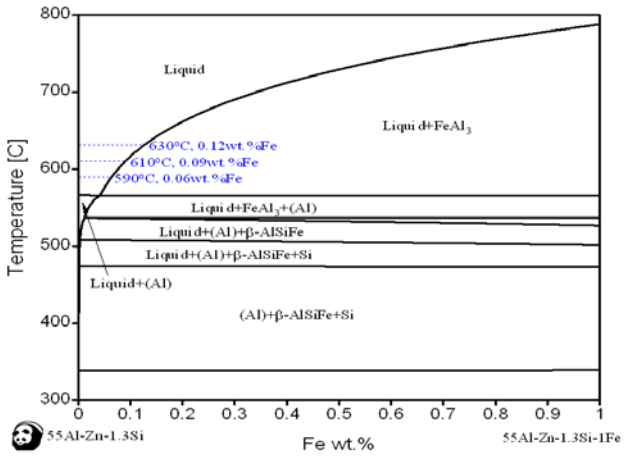


**Fig. 3.** The isoplethal section of Al-Zn-Si-Fe system from 55wt.%Al-Zn-1.3Si to 55wt.%Al-Zn-1.3Si-1Fe

Fig. 4 shows the calculated solidification path of the 55wt.%Al-Zn-1.3Si-0.13Fe alloy. It suggests that the $FeAl_3$ phase was firstly precipitated at 633 °C, then the liquid partly decomposed to become $FeAl_3$ and (Al) through eutectic reaction. The quasiperitectic reaction Liquid+$FeAl_3$→β-AlSiFe+(Al) occurred at 536 °C. Therefore, the β-AlSiFe phase nucleates and grows at the surface of $FeAl_3$ phase, which is in agreement with the result of Fig. 2(b). After the solidification, the dross is composed of $FeAl_3$, β-AlSiFe and (Al). The calculated phase compositions agreed well with the results of SEM and XRD.

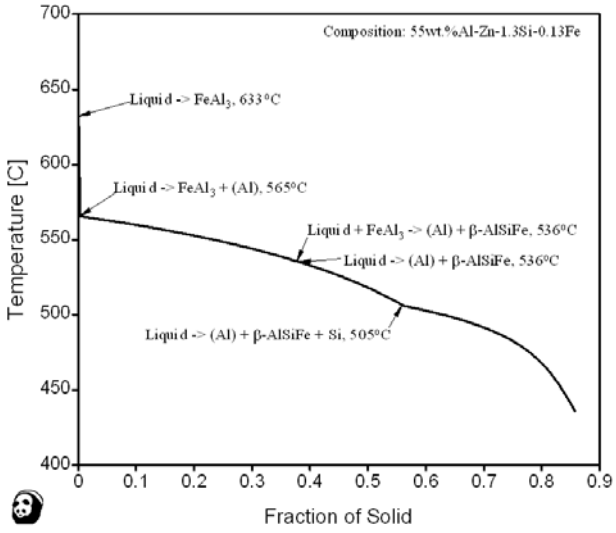


**Fig. 4.** The solidification path of the 55wt.%Al-Zn-1.3Si-0.13Fe alloy

The solution of Fe in molten alloy is unavoidable during continuous hot-dip galvanizing and continuous heat of the zinc bath. The large temperature fluctuations would lead to increasing of dross. Take the composition of 55wt.%Al-Zn-1.3Si-0.13Fe for example, 0.17 wt.% $FeAl_3$ will precipitate from the liquid when temperature decreases from 630 °C to 590 °C according to our calculation. At this moment the Fe level in liquid reduce to 0.06 wt.%. However, when bath temperature increases, the Fe will dissolve in the liquid continuously from steel

sheet and hot-dip equipment. And then if temperature decreases, the $FeAl_3$ will be produced again. This process repeating again and again leads to the formation of a large quantity of dross. Therefore, the bath temperature should be remaining steady in order to reduce the amount of dross formation.

### 4.2 The effect of Si content on the solubility of Fe in 55wt.%Al-Zn-Si molten alloy

In this work, the effect of Si content on the saturation solubility of Fe was analyzed by calculated Al-Zn-Si-Fe phase diagram. Fig. 5 shows the isothermal section on the Al-Zn rich side of the Al-Zn-Si-Fe system at 0.5 wt.% Si and 610 °C. The dash line and dotted line in Fig. 5 are the boundaries of liquid at 1.0 wt.% and 1.5 wt.% Si, respectively. It can be seen that the area of liquid enlarges with the increasing of Si content, which suggests that the saturation solubility of Fe increases with the increasing of Si content.

In order to illustrate the effect of Si content on the amount of dross formation, the saturation solubility of Fe in 55wt.%Al-Zn-0.5Si and 55wt.%Al-Zn-1.5Si molten alloy was calculated respectively. Table 3 shows the comparison of solubility of Fe in liquid and quantity of precipitated $FeAl_3$ at 0.5 wt.% and 1.5 wt.%. The decreasing of temperature from 630 °C to 590 °C leads to 0.14 wt.% $FeAl_3$ precipitating at 0.5 wt.% Si. However, at 1.5 wt.% Si the same temperature fall would produce 0.17 wt.% $FeAl_3$. In other words, the quantities of dross formation in low-Si molten alloy is less than that in high-Si molten alloy although the saturation solubility of Fe in high-Si melt is large than the former.

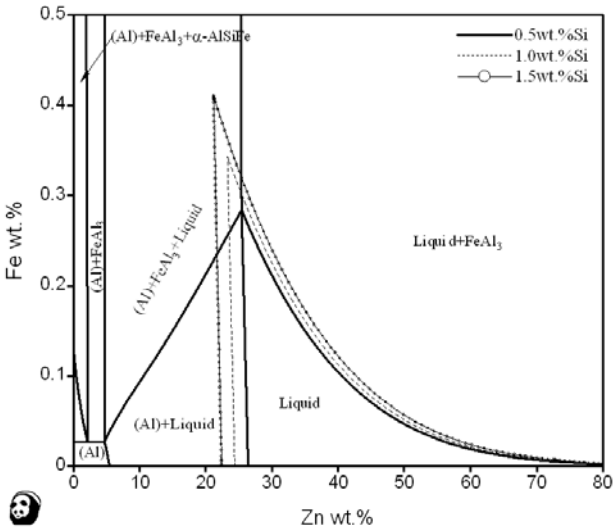


**Fig. 5.** The solubility curves of Fe in the liquid phase at 610 °C with different Si content

Table 3. The comparison of solubility of Fe in liquid and amount of precipitated $FeAl_3$ at different Si content

| Content of Si /wt.% | Saturation solubility of Fe /wt.% | | | Amount of precipitated $FeAl_3$ /wt.% |
|---|---|---|---|---|
| | 630°C | → | 590°C | |
| 0.5 | 0.10 | → | 0.05 | 0.14 |
| 1.5 | 0.13 | → | 0.07 | 0.17 |

## 5. Conclusions

The composition of hot-dip molten bath and phase composition of the bottom dross were determined by ICP, XRD and SEM. The reason of bottom dross formation was analyzed based on the Al-Zn-Si-Fe thermodynamic database constructed in our work group. The results obtained can be summarized as follows:

1. The XRD of the bottom dross showed that the main dross was the $FeAl_3$ phase. The SEM and EDS results proved that the $FeAl_3$ particles formed in dross, and a little β-AlSiFe grew on the edge of large $FeAl_3$ particle. In addition, a few Al-Zn-V intermetallic particles were found between the $FeAl_3$ particles.
2. The calculated values of Fe saturation solubility at 590~630 °C agreed well with the experimental data. With bath temperature deceasing from 630 to 590 °C the saturation solubility of Fe reduced from 0.12 wt.% to 0.06 wt.%. The bath temperature fluctuations would lead to increasing of bottom dross.
3. The saturation solubility of Fe in molten alloy increased with the rising of Si content from 0.5 wt.% to 1.5 wt.%. However, the amounts of dross formation in low-Si molten alloy are less than that in high-Si molten alloy at the same bath temperature fluctuations.

## Acknowledgements

The authors thank Instrumental Analysis and Research Center of Shanghai University for their support of materials testing and research. This work was financially supported by the National Natural Science Foundation of China (51074103), Chinese National Key Technology R & D Program (2007BAE09B03), Science and Technology Commission of Shanghai Municipality (10195802000) and Key Science and Technology Development Program in the Eleventh Five-Year Plan of Guizhou Province (20076003).

## References

[1] J. H. Selverian, M. R. Notis, A. R. Marder. The microstructure of 55 w/o Al-Zn-Si (Galvalume) hot dip coatings. Journal of Materials Engineering, 1987, 9(2): 133–140.

[2] L. Zhu. Brief introduction of the production of hot galvanized steel sheet. Aisc Techniques, 2000(1): 58–62, in Chinese.

[3] K. Tano, S. Higuchi. Development and properties of zinc-aluminum alloy coated steel sheet with high corrosion resistance (super zinc). Nippon Steel Technical Report, 1985, 25: 29–37.

[4] M. H. Ouyang, Z. Li, X. M. Wang, F. C. Yin, J. H. Wang, X. P. Su. Control of bottom dross in 55%Al-Zn bath. Materials Science and Engineering of Powder Metallurgy, 2008, 13(3): 139–144, in Chinese.

[5] D. J. Willis. Fluid flow modeling in a 55%Al-Zn pot: BAKER M A. Calvatech'04. Chicago: AIST, 2004: 905–916.

[6] D. J. Willis. Developments in hot dipped metallic coated steel processing. Materials Forum, 2005, 29(1): 9–16.

[7] S. Belisle, V. Lezon, M. Gagne. The solubility of iron in continuous hot-dip galvanizing baths. Journal of Phase Equilibria, 1991, 12(3): 259–265.

[8] Y. W. Kim, S. C. Kung, W. C. Sievert. Surface defects in exposed quality hot-dip galvanized steel: HISAMATSU S. Galvatech’89. Tokyo: The Iron & Steel Institute of Japan, 1989: 120.

[9] H. L. Miao. The control of bottom slag in band steel galvanizing. Hunan Nonferrous Metals, 2005, 21(1): 30–61, in chinese.

[10] X. B. Liu, H. C. Lin. Analyses of zinc pot roller slagging at Galvanized (GL). Metal World, 2010, 2: 37–39, in Chinese.

[11] A. Varadarajan. Dross formation mechanism and development of wear resistant scraper in 55Al-1.5Si-Zn coating bath, Ph.D thesis, West Viginia University, 2008.

[12] S. Shawki, Z. A. Hamid. Effect of aluminium content on the coating structure and dross formation in the hot-dip galvanizing process. Surface and Interface analysis, 2003, 35: 943–947.

[13] Q. Li, Y. H. Zhao, Y. Z. Zhao, F. Yang, J. Y. Zhang, K. C Chou, Y. Che, Z. K. Zhang. CN200820153902.9.